Implementation of PCC-OFDM on a software-defined radio testbed

Gayathri Kongara
Monash University

Jean Armstrong
Monash University

Abstract: A software-defined radio implementation of polynomial cancellation coded orthogonal frequency division multiplexing (PCC-OFDM) on a field programmable gate array (FPGA) based hardware platform is presented in this paper. Previous publications on PCC-OFDM have demonstrated that, in comparison to normal cyclic prefix based OFDM, it is robust in the presence of many impairments including carrier frequency offset, multipath distortion and phase noise. The error performance of the two multicarrier techniques is compared on a practical wireless channel under common channel impairments such as carrier frequency offset, multipath and noise. Based on the comparative results obtained on the hardware platform, the properties of PCC-OFDM make it a suitable candidate for consideration in future 5G applications requiring robust performance in asynchronous environments with minimal out of band spectral emissions.

Keywords: PCC-OFDM, software-defined radio, 5G waveforms

Introduction

Many new applications such as the Internet of things (IoT) and machine-type communications are envisaged to be integral to fifth generation (5G) communication systems. These new scenarios in next generation systems will pose challenges that include an increase in aggregate date rate by 1000 fold, a requirement for round trip latency less than 1ms, and support for asynchronous communications (Aminjavaheri, Farhang, RezazadehReyhani, & Farhang-Boroujeny, 2015). Cyclic prefix orthogonal frequency division multiplexing (CP-OFDM) at present is the most successful physical layer solution in 4G communication systems. Due to frequency domain based signal processing, implementation of CP-OFDM results in significantly lower computational complexity for dispersive channels than single carrier transmission which is traditionally combined with time domain based receiver signal processing. However, CP-OFDM in its basic form will not meet the diverse requirements of

http://doi.org/10.18080/ajtde.v5n2.98

future 5G scenarios (Aminjavaheri et al., 2015; Kténas, 2015). One of the major limitations of CP OFDM is that without subcarrier (individual or a group) filtering it has high out-of-band (OOB) emissions (Aminjavaheri et al., 2015; Fettweis, Krondorf, & Bittner, 2009). CP-OFDM is also known to be highly sensitive to time and frequency synchronisation errors. The performance of CP-OFDM with practical time and frequency synchronisation techniques can deviate significantly from that obtained in ideal channel conditions. In addition, the length of the CP required in high delay spread channels increases as the number of samples affected by the inter-symbol-interference (ISI) increases. In general, the transmitter and receiver carrier frequencies are generated by different local oscillator clocks which may not have the same frequency accuracy and hence a non-zero carrier frequency offset (CFO) manifests in the signal reception. CP-OFDM based 4G systems rely on tight time and frequency synchronization to achieve the required error performance. However, this may not be realistic in future 5G systems. Inaccurate synchronization coupled with mobility in the wireless channel (Doppler) can disrupt the orthogonality of the sub-carriers in OFDM systems ultimately deteriorating the overall error performance. In some applications such as machine type communications (MTC) in 5G, maintaining strictly synchronized transmission is not possible as it is throughput inefficient. Tolerance to some asynchronous operation is very important for a good system design for such applications.

A diverse range of applications envisioned for 5G networks require access to spectrum within three key frequency ranges which are sub- 1 GHz, 1-6 GHz and above 6 GHz (This includes spectrum above 24 GHz). Compared to 4G frequency bands, 5G networks use very high frequencies and hence suffer from higher losses. Although OFDM is the dominant PHY layer solution in 4G applications, some of its weaknesses such as sensitivity to frequency offset errors and higher OOB emissions may become major issues for use with future 5G systems. Hence, there is a growing interest from both industry and academia in exploring alternative waveforms to suit 5G. A summary of OFDM waveform alternatives that rely on filtering of sub-carriers for 5G scenarios are currently under 5G networks (Farhang-Boroujeny & Moradi, 2016).

Polynomial cancellation coded orthogonal frequency division multiplexing (PCC-OFDM) modulation technique has been shown to have better spectral characteristics resulting in significantly lower OOB emissions than the conventional OFDM systems (Armstrong, 1999) (Armstrong, Gill, & Tellambura, 2000; Shentu, Panta, & Armstrong, 2003). The complex data samples in PCC-OFDM are mapped onto groups of subcarriers rather than individual subcarriers as in CP-OFDM. For example, a grouping order of two with PCC means that each data sample is mapped onto a pair of adjacent subcarriers scaled by factors $+1$ and -1. The overall OOB spectral roll-off for PCC-OFDM increases with increase in the grouping

http://doi.org/10.18080/ajtde.v5n2.98

order, however, this is achieved at the cost of some decrease in the spectral efficiency (Armstrong, 1999). However, some other properties of PCC-OFDM can reduce the overall spectral loss. The CP required in conventional OFDM can be a significant overhead in high delay spread channels unlike conventional OFDM, does not need a CP.

Another way to increase the spectral efficiency of PCC-OFDM is to overlap symbols before data transmission. With this approach, ISI is deliberately introduced into the signal before transmission. A multi-stage equaliser at the receiver which operates as a linear, or decision feedback equaliser is then used to recover the signal (Armstrong et al., 2000).

A number of alternative schemes are currently under development. These mainly rely on filtering the subcarriers with special pulse shaping filters; it was shown that the required low OOB emissions for 5G could be achieved with the use of long filters (Aminjavaheri et al., 2015; Farhang-Boroujeny & Moradi, 2016; Kténas, 2015). Filtering of individual sub-carriers or a group of sub-carriers decreases signal to noise ratio (SNR) and adds to the end-to-end latency of the system. Other techniques that implement sophisticated interference cancellation at the receiver along with CFO compensation have been explored (Defeng & Letaief, 2005; Lee & Lee, 2011). Such techniques again add signal-processing complexity and latency. Filtering based multicarrier waveforms of (Aminjavaheri et al., 2015; Fettweis et al., 2009) were shown to provide significant improvement compared to conventional CP-OFDM systems.

In this paper, we describe a system implementation of PCC-OFDM on the USRP hardware. Since the introduction of PCC-OFDM in 1998-99 (Armstrong, 1999), a number of studies describing the theoretical and numerical performance limits under various propagation impairments have appeared in the literature. However, there are no publications on PCC with hardware implementation results. In this paper, we present a description of PCC-OFDM and CP-OFDM implementations on a software-defined radio (SDR) test platform. We introduce time and frequency errors in the experiments to compare their relative strengths and weaknesses.

The organisation of the paper is as follows. In Section 2, the software defined radio platform is described. Section 3 introduces the PCC-OFDM system model. Section 4 describes the receiver processing algorithm for the time and the frequency synchronisation. Channel estimation and equalisation are discussed in Section 4. Section 5 presents performance results from the hardware implementation of PCC and CP-OFDM under various propagation scenarios.

http://doi.org/10.18080/ajtde.v5n2.98

Software Defined Radio Platform

The SDR platform consists of one or more USRP 2943R devices that can be programmed as a transmitter or receiver. The USRPs connect to a personal computer (PC) running National Instruments (NI) LabVIEW 2016 as shown in the two configurations in Figure 1. The high-speed low latency PCIeX4 interface cards installed on the PC are capable of data transfer at 800 Mbps (NI, 2015). The PCIeX4 interface card loads compiled bit files from the LabVIEW environment on to the FPGA motherboard. This host-based LabVIEW system implementation offers great flexibility in the system design, configuration and testing. In addition to the entire physical layer signal processing in LabVIEW, RF system parameters can be configured in software. The transmitter (TX) is connected to the USRP RIO0 device's RF0 daughter board. The receiver (RX) is on either a RF1 daughter board of the same USRP RIO0 as shown in Figure 1 (a) or a physically separate device named USRP RIO1 that is connected to the same PC but placed at 1m distance away from the USRP RIO0 as shown in Figure 1 (b).

The frequency accuracy is usually specified in the hardware specification sheets. This is calculated from the frequency error normalised to the sampling rate. For USRP RIO 2943R, a ± 2.5 parts per million (ppm) frequency error can occur (NI, 2015). This means that the hardware introduces ± 2.5Hz frequency error for a 1MHz sampling rate. This is much smaller than the subcarrier spacing we use in our experiments. The data sheets of USRP-RIO indicate that the hardware introduces a delay of less than 1 μsec. Hence, hardware induced impairments are so small when experiments are conducted on the same device that frequency synchronisation is typically not necessary.

However, in experiments where the transmitter and receiver are separated by a distance 1m or greater, a significant time and frequency offsets affect the received signal. A correlation based two-stage time and frequency synchronisation algorithm is described in this paper. Performance results for PCC and CP-OFDM implementations with the synchronisation algorithm are compared for frequency offset in an AWGN channel and various modulation orders

PCC-OFDM System Model

The transmitter block diagram of the PCC-OFDM is illustrated in Figure 2. At the transmitter, information bits are modulated using 16-QAM and 64-QAM with PCC carrier grouping. A grouping order of two is assumed in this paper, so QAM modulated samples are mapped onto a weighted pair of adjacent subcarriers with a relative weighting of $+1, -1$.

http://doi.org/10.18080/ajtde.v5n2.98

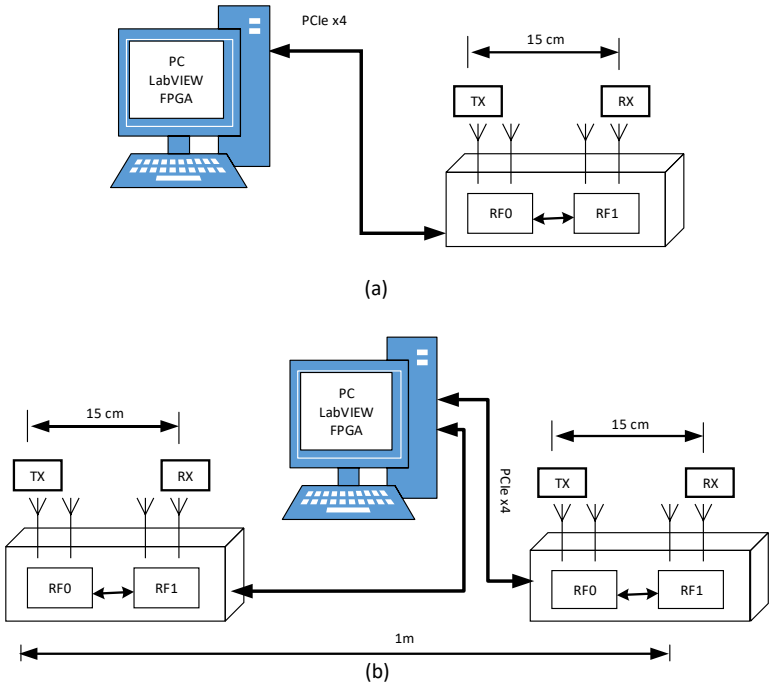

Figure 1: LabVIEW based Software Defined Radio Platform with (a) one USRP (b) two USRPs

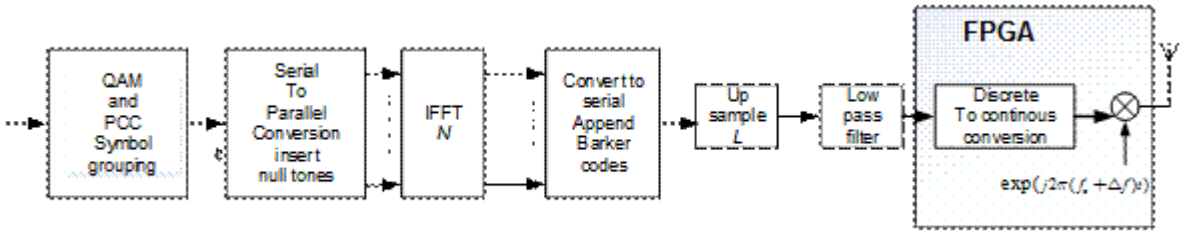

Figure 2: PCC OFDM Transmitter

A typical transmission frame carrying multiple OFDM or PCC symbols with Barker training sequences is shown in Figure 3. A repetition of training information induces periodicity into the transmission which the receiver uses in the estimation of CFO, delay and channel state information. Each training block is a Barker code which comprises a sequence of $+1$ or -1 and exhibits good aperiodic autocorrelation properties (Moose, 1994).

http://doi.org/10.18080/ajtde.v5n2.98

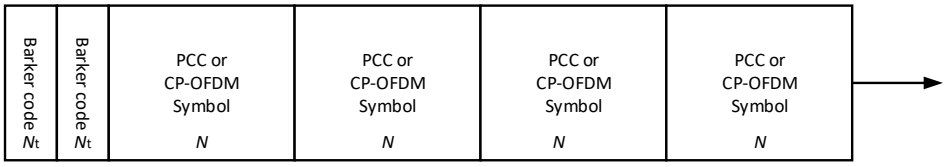

Figure 3 Transmission frame carrying PCC-OFDM symbols

The serial information QAM symbol stream is split into *N* parallel sub-streams that are mapped onto *N* subcarriers. The pair of subcarriers around Nyquist frequencies are nulled. Four subcarriers around zero frequency are further nulled as any DC bias complicates the analogue to digital and digital to analogue conversion processes. After the subcarrier nulling stage, the time domain data is generated using an inverse fast Fourier transform (IFFT). The parallel information streams are converted back into a serial data stream and up-sampled. This signal then passes through a band-limiting filter and then the RF front-end for digital-to analogue conversion and transmission across the wireless channel.

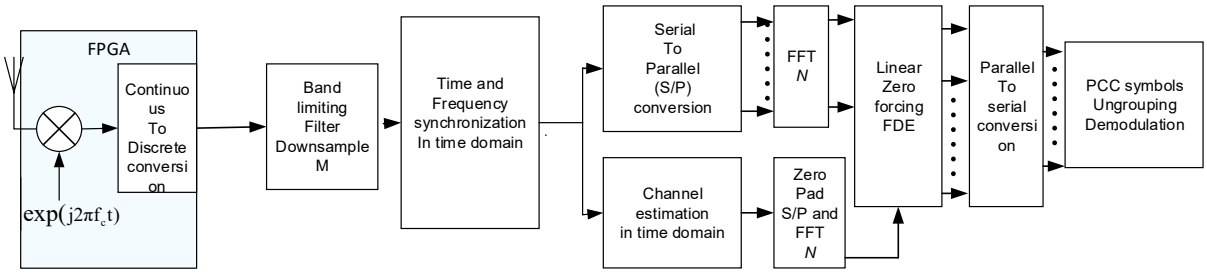

Figure 4 PCC OFDM Receiver

The block diagram of the implementation of the PCC-OFDM receiver is shown in Figure. 4. The time offset is denoted as *D*, multipath dispersion of the channel is defined by the vector $\mathbf{h} = \left[h(0),\ h(1),...h(p\ -\ 1)\right]$ and CFO by Δf. The CFO normalised to the sample period T is denoted by $\varepsilon = \Delta fT$. Given the transmit signal $x(n)$ (for the n^{th} discrete time instant) at the IFFT output, the received signal sample $y(n)$ is given by

$$y(n) = \exp(j2\pi\varepsilon n)\sum_{l=0}^{p-1} h(l)x(n-l-D) + \omega(n). \quad (1)$$

Where, $\omega(n)$ corresponds to the sample of AWGN and p is the multipath (wireless) channel order.

http://doi.org/10.18080/ajtde.v5n2.98

Time and frequency synchronisation

The delay parameter may span several symbol periods and must be estimated to determine the frame start. Prior to this, a fractional time synchronisation is carried out on the oversampled received frame. To achieve this the received OFDM or PCC signals are up-sampled with the same oversampling rate as was used at the transmitter. The calculation of the fine time synchronisation offset involves tracking the energy of the received frame over L fractional time delays where each delay is Ts/L. The time index corresponding to the maximum energy of the received frame is used to compensate the fractional time offset. The fine synchronisation results in a sample level signal that has an integer time offset. This is carried out at a sample level following fine synchronisation process. A simple correlation-based peak-detection technique is used to estimate the unknown integer delay. To estimate the integer time offset, the received signal corresponding to the training phase is correlated with the training signal given by

$$\mathrm{R}(n) = \left\| \sum_{k=0}^{N_t-1} t^*(k)\, y(n+k) \right\|^2, \tag{2}$$

where N_t is the length of the training sequence. An estimate of the delay parameter D in (1) is then calculated by taking the index n of the maximum value of the correlation metric given in (2). This is given by

$$\hat{D} = arg\left(\max_{\mathrm{n}} \mathrm{R}(n) \right) \tag{3}$$

The frame start is set to the estimated integer delay parameter $\hat{D}$ to compensate for the overall delay in transmission. However, in the presence of CFO, the correlation peak may be erroneously shifted due to ICI. For small estimation errors, a simple one-tap linear equaliser can be used to compensate for the offset. However, in the presence of significant CFO, the frequency error should be properly estimated and compensated for before carrying out further receive processing. After frame synchronisation using $\hat{D}$ the received signal in (1) reduces to

$$y(n) = \exp(j2\pi\varepsilon n) \sum_{l=0}^{p-1} h(l)x(n-l) + \omega(n), \tag{4}$$

The next step is to estimate the frequency error $\varepsilon = \Delta fT$. Noticing that the two received blocks corresponding to the consecutively transmitted training blocks each of length N_t differ by a phase of $\exp(j2\pi N_t\varepsilon)$, we formulate a least-squares problem. For brevity, we denote $\exp(j2\pi N_t\varepsilon) = a$ and the objective function is written as

http://doi.org/10.18080/ajtde.v5n2.98

$$J(a) = \sum_{n=0}^{Nt-1} \| y(n + N_t) - a y(n) \|^2 . \quad (5)$$

Minimisation of the metric defined in (5) results in

$$\hat{a} = \frac{\sum_{n=p}^{Nt-1} y(n + N_t)\, y^*(n)}{\sum_{n=p}^{Nt-1} \| y(n + N_t) \|^2} \quad (6)$$

In (6), the first few training samples affected by channel memory are discarded when calculating the synchronisation parameters. The normalised CFO estimate is simply the angle of (6) which is given by:

$$\hat{\varepsilon} = \angle \left(\frac{\sum_{n=p}^{Nt-1} y(n + N_t)\, y^*(n)}{2\pi N_t} \right) \quad (7)$$

The estimated $\hat{a}$ is used in compensating the CFO at the receiver, by multiplying by the received frame with $\hat{a} = \exp(-2\pi N_t \hat{\varepsilon})$. Synchronisation is followed by channel estimation and equalisation based on the training vector $t = \left[t(0),\ t(1),\ \ldots,\ t(N_t - 1) \right]$. The time domain signal after time and frequency synchronisation is given by

$$y(n) = \sum_{l=0}^{p-1} h(l)\, t(n-l) + w(n) \qquad n = [0,\ 1,\ \ldots, N_t - 1] \quad (8)$$

The channel effect in (8) should first be estimated. A simple and practical channel estimation algorithm based on the linear least squares (LS) criterion is employed. Unlike minimum mean squared error (MMSE) estimation approaches, LS does not require accurate real-time estimates of noise at the receiver. Channel estimates are calculated upon minimising the error between the received samples and the training samples ignoring the effect of additive noise. Hence, this approach has a disadvantage in high noise conditions where an implementation of MMSE channel estimates gives inaccurate estimates. The estimated channel coefficients in the time domain give the time domain equaliser parameters. The frequency domain equaliser (FDE) is calculated by Fourier transformation of the time domain channel parameters. A direct time domain approach to calculation of equaliser parameters is obtained by forming an error metric from the training and the estimated samples. The equaliser vector is calculated by

http://doi.org/10.18080/ajtde.v5n2.98

$$\mathbf{f} = (\bar{\mathbf{y}}^{*}\ \bar{\mathbf{y}})^{-1}\ \bar{\mathbf{y}}\mathbf{t} \tag{9}$$

where $\bar{\mathbf{y}}$ is a matrix of dimension $(N_t + 1)x\ (L + 1)$ and $\mathbf{f}$ is the equaliser vector with L taps of dimension $(L + 1)x1$. The discrete Fourier transform of (9) gives the FDE $\boldsymbol{F} = [\,F(0), F(1), \ldots, F(N\ -\ 1)]$. A simple zero-forcing FDE is implemented to compensate for the distortion due to multipath which is given by

$$X(k)\ = \frac{Y(k)}{F(k)} \qquad k\ =\ [0,\ 1,\ \ldots, N]. \tag{10}$$

After FDE, for PCC, the grouped subcarriers are de-multiplexed and decoded for data recovery and BER is calculation. In the following section hardware results are presented for the receiver described in this section.

Hardware Results

In this paper, we extend the experiments reported in our previous papers (Kongara & Armstrong, 2016, 2017) in which a performance comparison of the hardware implementations of PCC-OFDM and CP-OFDM with $4-$QAM was presented. To investigate the effects of CFO and multipath, we consider two experimental set-ups as illustrated in Figure 1. In Figure 1 (a) the physical separation of transmitter and receiver is 15 cm as they are connected to the same USRP. The set-up in Figure 1 (b) has transmitter and receiver on different devices but the range is restricted to 1m as both devices are connected to the same PC. The focus of our current work is comparing the robustness of the two modulation schemes in real wireless channels. Increasing the range to more than a meter is possible but is outside the scope of our current investigation.
In the current paper, experimental results for the hardware configuration shown in Figure 1 for 16-QAM and a 64-QAM formats are discussed. In all our experiments, a carrier frequency in the Industrial Scientific and Medical (ISM) band (2.41 GHz) and an antenna gain of 10 are used. A traditional time domain approach to synchronisation and channel estimation (see Section 4 above) is employed and hardware performance of the two systems is compared. The need for more accurate time synchronisation for 64-QAM compared to 16-QAM and 4-QAM schemes is discussed. We then compare the BER performance of the time and frequency synchronised PCC and OFDM systems under variable AWGN conditions, CFO, FFT sizes and transmission frame lengths. Both instantaneous and average results are used in understanding and drawing conclusions on the robustness of PCC system against normal OFDM system.

Experiments are conducted on a SDR platform with the transmitter and receiver separated by a distance of 15 cm (shown in Figure 1 (a)) and 1 metre (shown in Figure

http://doi.org/10.18080/ajtde.v5n2.98

1 (*b*)). We first investigate the requirement for oversampling to enable initial timing estimation by tracking the output energy of the detector described in Section 4. Each transmission frame is approximately 4 ms in duration and carries 12k and 24k information bits for the PCC-OFDM and CP-OFDM schemes, respectively. For 64-QAM and N=1024, the transmission frame carries 4 symbols modulated using either PCC or normal CP-OFDM symbols.

In Figure 5 (*a*) we see an example of a transmission frame containing the time domain PCC-OFDM symbols after IFFT operation that is generated with an FFT size of N=1024. The received constellation corresponding to the transmission of Figure 5 (*a*) is shown in Figure 5(*b*). Figure 5 (*c*) and (*d*) illustrate the OFDM transmit waveform and received constellation. A subcarrier grouping order of 2 is used for PCC-OFDM symbols in this paper. As can be seen in Figure 5 (*a*), due to the PCC coding, the symbol transitions are smooth with an effect of time domain windowing. This time domain symbol shape achieved with PCC grouping is shown to be equivalent to filtering with a Hanning window (Panta & Armstrong, 2003). The OFDM waveform without additional filtering has sharp transitions compared to PCC-OFDM. This results in higher out of band emissions for OFDM compared to that for PCC system. The spectral efficiency of PCC is halved due to the sub-carrier grouping. However, a CP length equal to a quarter of the symbol period is generally needed for OFDM to eliminate ISI. Whereas PCC is more tolerant to multipath propagation

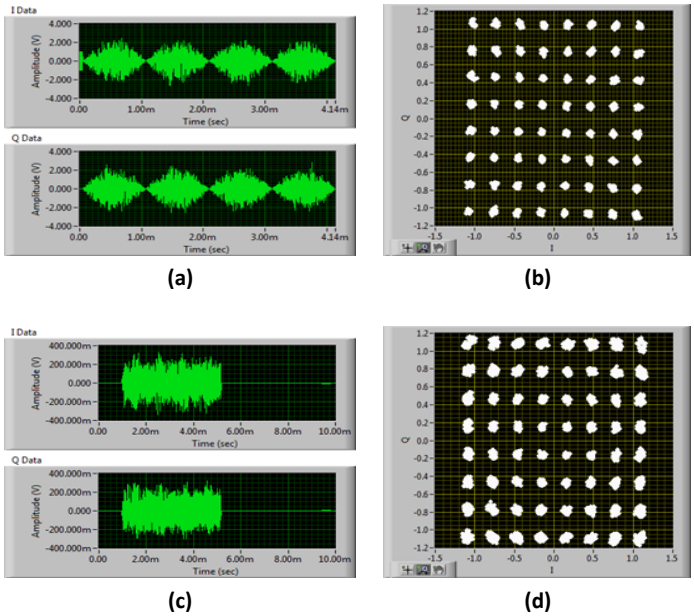

Figure 5: (a) I and Q components of the transmission frame carrying four PCC-OFDM symbols of 64QAM samples. (b) Received constellation corresponding to (a) over the wireless channel. (c) I and Q components of

http://doi.org/10.18080/ajtde.v5n2.98

a transmission frame carrying four CP-OFDM symbols of 64QAM samples. (d) Received constellation corresponding to (c) over the wireless channel.

In Figure 6, examples of the received constellations that correspond to the transmission of PCC-OFDM symbols carrying QPSK, 16-QAM and 64-QAM data are shown for an oversampling factor of 2. The average BER calculated from over 100 transmission frames result in a BER= 0 for 4-QAM . However, an average BER = 0.006185 for 16 QAM and BER =0.022 for 64-QAM is obtained on the real wireless channel with clear line-of-sight. As seen from the constellations, higher order modulations such as 16-QAM and 64-QAM demand more precise estimates for the timing information at the receiver.

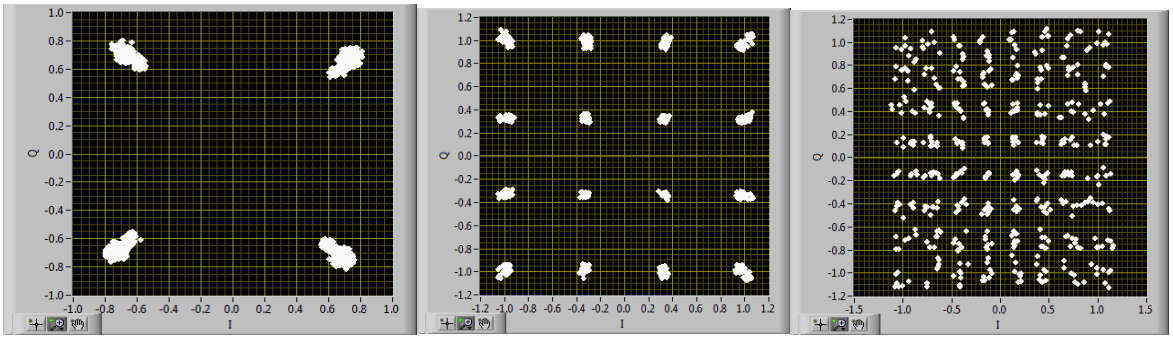

(a) QPSK samples **(b) 16-QAM samples** **(c) 16-QAM samples**

Figure 6: Received constellation with an oversampling factor of 2 corresponding to the transmission of PCC frame carrying (a) QPSK samples (b) 16-QAM samples (c) 64-QAM samples.

In our hardware implementation, we used an oversampling approach similar to (Awoseyila, Kasparis, & Evans, 2009) to calculate more precise sampling instants. This approach is based on tracking the energy of the received frame over a certain range of delays. A sliding window is used that outputs the energy of the received frame for every sample delay. The tracking process continues until it finds the sample delay that corresponds to the maximum output energy. In Figure 7, the output energy for oversampling factors of L=M=2, 4 and 10 are illustrated. As can be seen from the plots, the constellations with higher oversampling factors result in more precise sample time offset. However, it should be noted that choosing higher oversampling factors consumes more hardware resources and a trade-off between the complexity and required accuracy for a system should be carefully considered.

http://doi.org/10.18080/ajtde.v5n2.98

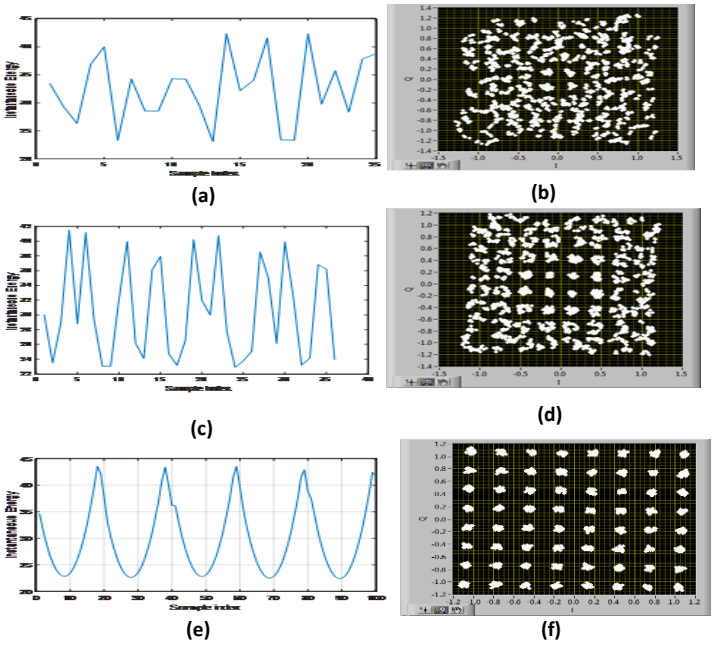

Figure 7: Output of the sliding energy detector with oversampling factor (a) L=M=2 (b) L=M=4 (c) L=M=10

In Figure 8, BER averaged over 100 channel realisations of transmission is plotted for a varying SNR. The experiment is over a real wireless channel with the transmitter and the receiver connected as in Figure 1 (a) to the same USRP device and sharing a common clock (no CFO). The channel is clear line of sight, and hence the channel estimator is programmed to estimate just one coefficient to compensate for fading in the line of sight path. Zero-forcing based FDE is calculated from the estimated channel and the signal is equalised in the frequency domain. The BER performance of PCC OFDM system is significantly better than the normal OFDM with a 4dB SNR improvement with good time synchronisation achieved with an oversampling factor of $L = M = 10$. However, a performance degradation is seen due to inaccurate timing synchronisation when $L = M = 2$ and 4 are used.

OFDM transmission through a fading wireless channel can disrupt the orthogonality of sub-carriers generating ICI and ISI. This makes the OFDM signal reception sensitive to frequency synchronisation errors. The CFO is estimated as described in Section 4 using the received transmission frames of a PCC or a normal OFDM.

Another important factor that can affect the average BER is the FFT size. In Figure 9(a) and (b) transmission frames with $N = 64$, and $N = 1024$ carrying PCC symbols is shown. The average BER with $N = 64$, and $N = 1024$ for PCC and OFDM is illustrated. With no added AWGN, the PCC scheme exhibits lowest average BER for $N = 1024$. Comparing PCC N=1024 with OFDM for a CFO range of 100Hz to 400Hz, OFDM performance is poorer than the former. A similar observation can be made from the performance obtained for $N = 64$. The

http://doi.org/10.18080/ajtde.v5n2.98

performance degradation for a smaller FFT size with $N = 64$ is more for the OFDM system compared to PCC. There is some loss in PCC performance with smaller FFT size of $N = 64$ compared to $N = 1024$. However, OFDM with $N = 1024$ is slightly worse than PCC with $N = 64$. This means that the CFO estimation error degrades OFDM more than PCC.

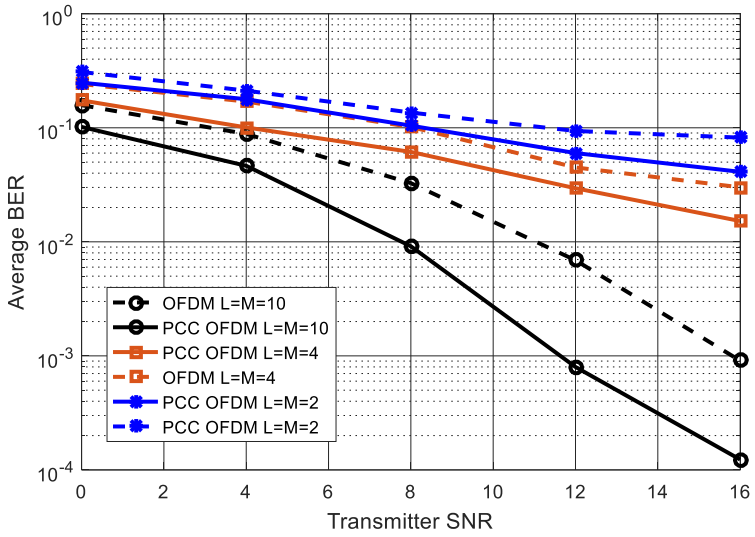

Figure 8 Transmit SNR versus BER comparison of PCC-OFDM against CP-OFDM for varying oversampling values.

As noise can further degrade performance, the performance at various SNR and CFO are studied in Figure 10. One observation from the results shown in Figure 10 is that for SNR =15, 20 and no noise conditions and under different values of CFO scenarios, PCC significantly outperforms normal OFDM. However, for higher values of CFO, both OFDM and PCC result degraded error performance.

In the next experiment, we look at the effect of long transmission frames on the achieved BER performance. The separation distance between the transmitter and receiver is set to 1m and the transmitter and receiver are on two separate USRP devices. The experimental set-up is as shown in Figure 1 (b). Transmission frame time with the test set-up of Figure 1(b) is $1/6^{th}$ of the frame duration that of Figure 1 (a). This is because, for increased path lengths, the channel state information changes significantly over the duration of the transmission frame and the synchronisation and channel parameters estimated at the start of the frame can be outdated for processing long frames.

http://doi.org/10.18080/ajtde.v5n2.98

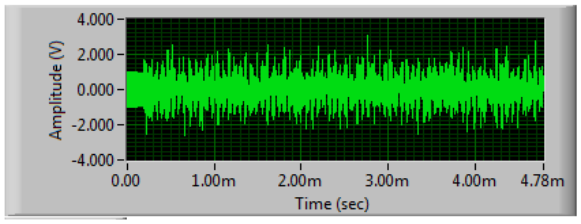

(a)

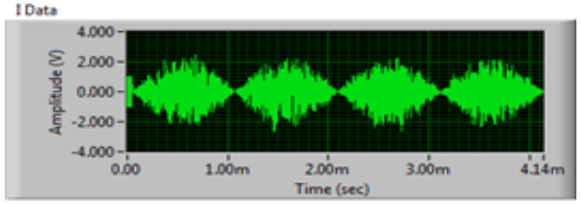

(b)

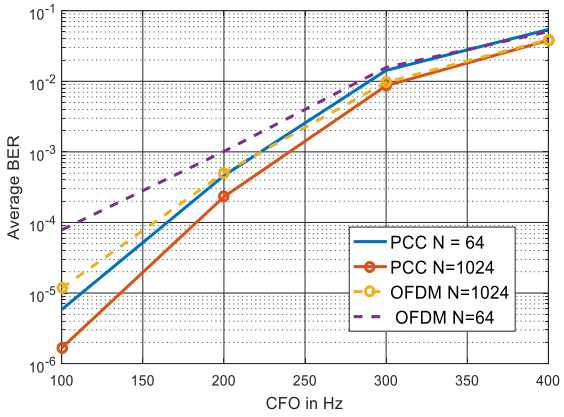

(c)

Figure 9: A transmission frame with PCC-OFDM 64 QAM samples (a) FFT size $N = 64$ (b) FFT size *N=1024* (c) Average BER vs CFO in Hz for PCC and OFDM of (a) and (b).

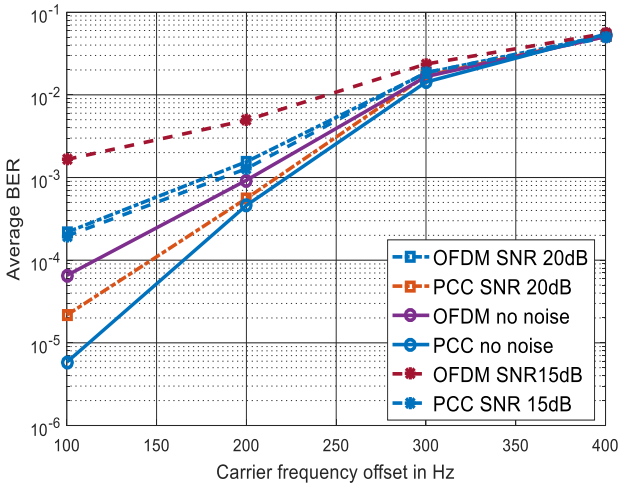

Figure 10. Average BER for comparison of PCC-OFDM against CP-OFDM for block FFT size *N=64* and SNR = 15 and 20. BER performance of the hardware with no additional noise is also shown for comparison.

http://doi.org/10.18080/ajtde.v5n2.98

In Figure 11, instantaneous observations of the received frames after synchonisation and FDE for frames carrying 16-QAM and 64-QAM samples are plotted for smaller frame duration of 660μsec. In Figure 12, the average BER calculated from 100 transmission frames of PCC and OFDM with varying number of symbols carried in each frame is shown. As expected, the BER performance of PCC is an order of a magnitude better than the normal OFDM system. As the transmission frame duration increases, BER performance of both systems degrade. However, PCC outperforms OFDM for all frame durations considered in hardware experiments. The correlation based time synchronisation algorithm discussed in Section 4 compensates for the delay introduced by the wireless channel but the performance degrades with increase in frame duration (indicated by increase in number of symbols). As the frame size increases, indoor wireless propagation induces more ISI and more frequent receiver parameter estimation is required to compensate the detrimental effects due to ICI and ISI.

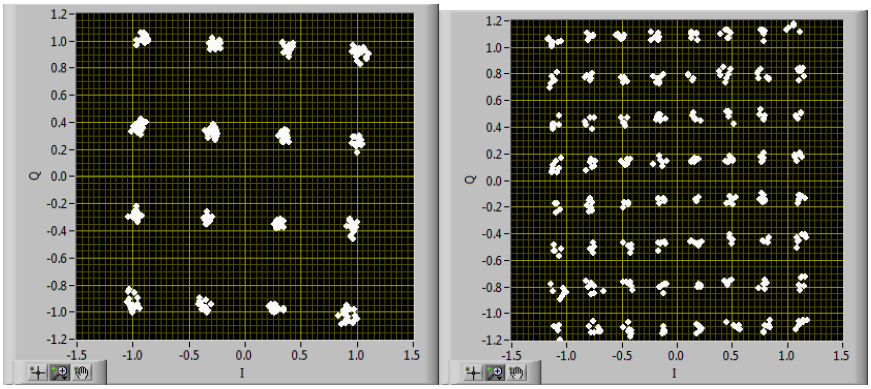

Figure 11 Instantaneous observations of transmission over 1m wireless channel after CFO compensation and equalisation

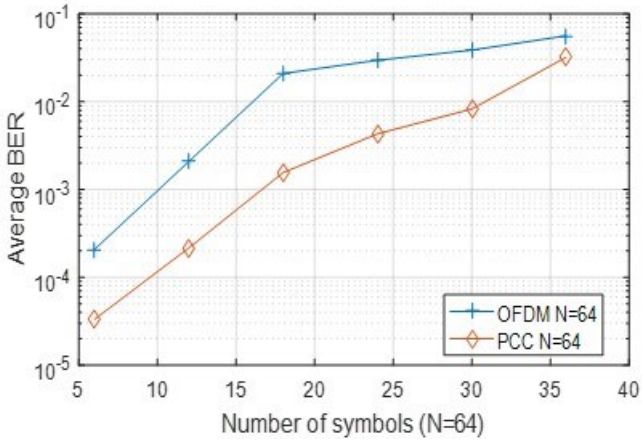

Figure 12. Average BER comparisons of PCC and OFDM symbols carrying 16 QAM samples over 1m wireless channel.

http://doi.org/10.18080/ajtde.v5n2.98

Conclusions

A hardware implementation of PCC-OFDM and CP-OFDM with symbols with 16-QAM and 64-QAM samples is presented in this paper. BER results from the hardware implementation of the two multicarrier approaches on USRP based SDR platform under variable channel impairments are compared. Hardware experimental results demonstrate the robustness of PCC-OFDM to time and frequency estimation errors under various noise conditions. A simple time domain correlation based timing and CFO estimation algorithm is implemented in LabVIEW to synchronise both systems. The hardware received time domain waveform of PCC-OFDM has smoother transitions resulting in lower OOB emissions than CP-OFDM. This is a major requirement for 5G systems. The performance degradation due to increased noise level for PCC is 3 – 4dB less than normal OFDM. The effect of smaller FFT size affects PCC less than OFDM. Experiments conducted on a wireless channel with a separation distance of 1 m show that the wireless channel introduces ICI and ISI in the received signals of PCC and OFDM. After synchronisation and equalisation, BER of PCC and OFDM compared under variable frame duration. PCC outperforms OFDM in for all frame sizes.

Acknowledgements

The authors wish to thank engineers at National Instruments for providing technical support on the SDR platform and Dr. Michael Biggar for sharing helpful comments and suggestions.

References

Aminjavaheri, A; Farhang, A; RezazadehReyhani, A; Farhang-Boroujeny, B. (2015). "Impact of timing and frequency offsets on multicarrier waveform candidates for 5G". Paper presented at the 2015 IEEE Signal Processing and Signal Processing Education Workshop (SP/SPE), 9-12 Aug. 2015.

Armstrong, J. (1999). "Analysis of new and existing methods of reducing intercarrier interference due to carrier frequency offset in OFDM". *IEEE Transactions on Communications*, 47(3), 365-369. doi: 10.1109/26.752816

Armstrong, J; Gill, T; Tellambura, C. (2000). "Performance of PCC-OFDM with overlapping symbol periods in a multipath channel". Paper presented at the Global Telecommunications Conference, 2000. GLOBECOM '00. IEEE.

Awoseyila, A. B; Kasparis, C; Evans, B. G. (2009). "Robust time-domain timing and frequency synchronization for OFDM systems". *IEEE Transactions on Consumer Electronics,* 55(2), 391-399. doi: 10.1109/TCE. 2009.5174399

Defeng, H; Letaief, K. B. (2005). "An interference-cancellation scheme for carrier frequency offsets correction in OFDMA systems". *IEEE Transactions on Communications,* 53(7), 1155-1165. doi: 10.1109/TCOMM.2005.851558

Farhang-Boroujeny, B; Moradi, H. (2016). "OFDM Inspired Waveforms for 5G".

IEEE Communications Surveys & Tutorials, 18(4), 2474-2492. doi: 10.1109/COMST.2016.2565566

Fettweis, G; Krondorf, M; Bittner, S. (2009). "GFDM - Generalized Frequency Division Multiplexing". Paper presented at the VTC Spring 2009 - IEEE 69th Vehicular Technology Conference 26-29 April 2009.

Kedia, M. (2005). "A computationally efficient method for estimating the channel impulse response for the IEEE 802.11b (WLAN)". Paper presented at the PACRIM. 2005 IEEE Pacific Rim Conference on Communications, Computers and signal Processing, 24-26 Aug. 2005.

Kongara, G; Armstrong, J. (2016). "Implementation of PCC OFDM on a software defined radio platform". Paper presented at the 2016 26th International Telecommunication Networks and Applications Conference (ITNAC), 7-9 Dec. 2016.

Kongara, G; Armstrong, J. (2017). "Performance evaluation of PCC OFDM on a software defined radio platform". Paper presented at the 2017 International Conference on Computing, Networking and Communications (ICNC), 26-29 Jan. 2017.

Kténas, D. (2015). 5G NOW: Final Assessment of Demonstrator Concept and Implementation

Lee, K; Lee, I. (2011). "CFO Compensation for Uplink OFDMA Systems with Conjugated Gradient". Paper presented at the 2011 IEEE International Conference on Communications (ICC) 5-9 June 2011.

Moose, P. H. (1994). "A technique for orthogonal frequency division multiplexing frequency offset correction". *IEEE Transactions on Communications, 42*(10), 2908-2914. doi: 10.1109/26.328961

National Instruments. (2015). Overview of the NI USRP RIO Software Defined Radio.

Panta, K; Armstrong, J. (2003). "Spectral analysis of OFDM signals and its improvement by polynomial cancellation coding". *IEEE Transactions on Consumer Electronics, 49*(4), 939-943. doi: 10.1109/TCE.2003.1261178

Shentu, J; Panta, K; Armstrong, J. (2003). "Effects of phase noise on performance of OFDM systems using an ICI cancellation scheme". *IEEE Transactions on Broadcasting, 49*(2), 221-224. doi: 10.1109/TBC.2003.810074

http://doi.org/10.18080/ajtde.v5n2.98